JOURNAL OF GEOPHYSICAL RESEARCH, VOL. 114, D10307, doi:10.1029/2008JD010155, 2009



# Information-centered representation of retrievals with limited degrees of freedom for signal: Application to methane from the Tropospheric Emission Spectrometer

Vivienne H. Payne,[1] Shepard A. Clough,[2] Mark W. Shephard,[1] Ray Nassar,[3] and Jennifer A. Logan[4]

Received 20 March 2008; revised 27 February 2009; accepted 16 March 2009; published 27 May 2009.

[1] Remote measurements of trace gas profiles from nadir-viewing instruments are often retrieved and/or reported on a fine grid containing more levels than the number of independent pieces of information in the measurement. Such profiles contain a priori information, which complicates interpretation. For scientific analyses of these data it is desirable to move to a representation in which measurement information is dominant and the influence of a priori information is minimal. Presented here is a postprocessing approach using a simple algorithm to transform each retrieved profile to an appropriate, geographically varying coarse grid. The representation is chosen such that the averaging kernel is close to unity for regions of the atmosphere where the retrieval has most information. The approach takes advantage of the sensitivity characterization allowed by retrieval on a fine grid, while reducing the influence of the a priori, accounting for spatial and temporal variations in the sensitivity of the measurement to the true atmosphere, and preserving obvious physical meaning in the end product. The example used to demonstrate the approach is the methane product from the Tropospheric Emission Spectrometer (TES), which contains 0.5–2.0 degrees of freedom for signal, depending on season and location. The TES methane has been postprocessed, and the end product has been compared with results from GEOS-Chem, a global chemical model. Results show realistic latitudinal gradients from the TES data. Model/measurement differences also show large-scale features over Indonesia that we attribute to tropical biomass burning in the summer/fall.

**Citation:** Payne, V. H., S. A. Clough, M. W. Shephard, R. Nassar, and J. A. Logan (2009), Information-centered representation of retrievals with limited degrees of freedom for signal: Application to methane from the Tropospheric Emission Spectrometer, *J. Geophys. Res.*, *114*, D10307, doi:10.1029/2008JD010155.

## 1. Introduction

[2] Methods used in remote sensing for atmospheric research often rely on information theory [*Rodgers*, 2000]. Such retrievals can be characterized by the number of degrees of freedom for signal (DOFS), i.e., the number of independent pieces of information in the measurement. For any given instrument and measurement technique, the amount of available information and the vertical distribution of this information vary according to the atmospheric state (temperature, trace gas concentration, clouds) as well as to the surface conditions (temperature, emissivity) for down-looking instruments.

[3] It is common practice to represent the state parameter to be retrieved on an altitude grid that is finer than the altitude resolution of the instrument [e.g., *Bowman et al.*, 2006; *Deeter et al.*, 2003; *von Clarmann et al.*, 2003]. A major advantage of this approach is that it allows the calculation of diagnostics, such as averaging kernels, which can be used to characterize the spatial and temporal variation in the sensitivity of the measurement. The use of a generic fine altitude grid is particularly relevant for the processing of satellite measurements, where the retrieval approach must be applicable to the range of conditions encountered on a global scale. Constraints must then be applied in order to stabilize the retrieval [e.g., *Rodgers*, 2000; *Tikhonov*, 1963; *Twomey*, 1963; *Steck and von Clarmann*, 2001; *Kulawik et al.*, 2006b]. In general, the constraints include both a constraint vector and a constraint matrix, which may be chosen in various ways to constrain absolute values and/or the shape of the retrieved result. This is of particular importance for nadir retrievals, where the vertical resolution is limited. The main disadvantage associated with

[1] Atmospheric and Environmental Research, Inc., Lexington, Massachusetts, USA.
[2] Clough Radiation Associates, Lexington, Massachusetts, USA.
[3] Centre for Global Change Science, University of Toronto, Toronto, Ontario, Canada.
[4] School of Engineering and Applied Sciences, Harvard University, Cambridge, Massachusetts, USA.


0148-0227/09/2008JD010155$09.00

the use of such constraints is that the solution of the retrieval problem does not then depend only on the measurement but also on the constraints used. This manifests itself not only in applications like quantitative validation of remotely sensed data, but even in the visual inspection of such data. The a priori constraints are often chosen to vary with space and time, in order to properly reflect the a priori knowledge of the atmospheric state. Such an approach was adopted for Tropospheric Emission Spectrometer (TES) retrievals described below. However, this introduces difficulty in distinguishing whether spatial structure and/or temporal variations in the retrieved product are related to changes in the constraints or to changes in the true atmospheric state. An alternative approach is to use a set of a priori constraints that is uniform in space and/or time, as adopted for MOPITT [*Deeter et al.*, 2003]. In most cases a globally uniform set of constraints clearly does not represent the best knowledge of the state available before the measurement. However, under certain circumstances the application of uniform constraints in postprocessing has been used to aid scientific interpretation of data. For instance, the application of a uniform constraint vector has been used in postprocessing of TES retrievals for the purposes of scientific analysis. Examples include analysis of differences between measurements and models, highlighting seasonal cycles and comparing observations from two geographical regions with different priors or comparing results from different satellite instruments [*Kulawik et al.*, 2008, and references therein]. *Kulawik et al.* [2008] have recently shown that this approach in postprocessing is valid. However, the use of a uniform a priori constraint vector can introduce biases that make some types of scientific analysis, such as the analysis of latitudinal gradients, difficult. Also, while the use of a globally uniform constraint vector and constraint matrix at least means that any structure or variations observed in the retrieved field must be due to information from the measurement, a uniform set of constraints does not lead to uniform a priori content in the retrievals, since the sensitivity of the retrieved profile to the true state (and therefore the extent to which the retrieval is influenced by the a priori constraints) depends also on the atmospheric and surface state. Therefore the biases cannot be assumed to be uniform, and so issues of interpretation remain.

[4] For certain types of scientific data analysis, it is advantageous, even critical, to utilize a representation of the retrieved state parameters in which the influence of the a priori constraints is minimal. In order to eliminate the influence of the a priori constraints as far as possible, the retrieved state should be reported in terms of one element per DOFS. Singular value decomposition-based approaches have been developed for the purpose of removing a priori influence from the data. *Ceccherini et al.* [2003] proposed such an approach for validation purposes targeted at maximum likelihood estimates of the atmospheric state. *Joiner and de Silva* [1998] proposed two methods: null-space filtering of retrievals and partial eigen-decomposition retrievals. These methods are rigorous and preserve the full information content of the measurements. However, the disadvantage of these approaches is that they transform the estimated state variables into a space without obvious physical meaning. *Pan et al.* [1998], in presenting an analysis of the information content of nadir CO retrievals, discuss an eigenvector analysis of the averaging kernels from optimal estimation retrievals in geophysical space. The leading eigenvectors for any given profile retain the full vertical resolution of the original product and typically have simple shapes that may be physically interpreted. Nonetheless, the interpretation of a large data set of such eigenvectors would not be intuitive, and the transformation of the state vector itself still results in an end result that is no longer in geophysical space.

[5] *Von Clarmann and Grabowski* [2007] proposed an approach targeted at a physically obvious representation of retrieved data that can be directly used and easily interpreted involving reregularization of the retrieval on a coarser grid. The retrieval is performed on the fine grid and then the results are postprocessed by mapping to a coarse grid that better represents the number of degrees of freedom for the retrieval. The number of useful grid points can be obtained by singular value decomposition, but not their vertical placement. The retrieval is transformed to an ''information-centered'' grid where each data point represents one degree of freedom. If the number of degrees of freedom is equal to the dimension of the retrieval vector, the a priori information is removed from the retrieval. Von Clarmann and Grabowski demonstrated their technique with a case study using stratospheric/upper tropospheric limb sounder data, where the DOFS is of the order of 9 to 10. With their approach, the retrieval can be regridded and reregularized to a representation where the a priori influence is completely removed and the number of degrees of freedom is reduced only to the next lowest integer value.

[6] The aim of this work is to apply an information centered postretrieval approach to tropospheric nadir retrievals where the degrees of freedom for signal is not significantly greater than (and may in fact be less than) 1.0. An approach is provided here for use of this type of satellite data for comparison with other data or with global models without the use of sophisticated data assimilation systems. The goals are (1) to reduce the influence of the a priori constraint on the end product, (2) to account for the spatial and temporal variations in the sensitivity of the measurement to the true state, and (3) to preserve obvious physical meaning in the end product. The example used to demonstrate the approach is the methane product from the Tropospheric Emission Spectrometer (TES) on the NASA Aura satellite, which contains between 0.5 and 2.0 DOFS, depending on season and geographical location. However, the general method is applicable to other data products and instruments.

[7] Section 2 provides an introduction to the TES methane retrievals. Section 3 outlines the postprocessing approach adopted to produce an end product that better represents the number of DOFS available, while preserving the information on the location of sensitivity of the measurement. Section 4 gives results, with a discussion of some preliminary scientific analysis involving comparisons with a global chemical model, in order to demonstrate the utility of the approach. It is shown that the application of this approach to the TES methane product allows an assessment of latitudinal gradients (which are small) as well as analysis of spatial features

in the model/measurement differences that suggest enhanced emission of methane associated with biomass burning.

## 2. Methane From the Tropospheric Emission Spectrometer

[8] Methane ($CH_4$) is an important greenhouse gas and plays a crucial role in tropospheric chemistry. Oxidation of $CH_4$ by hydroxyl radicals (OH) removes OH from the atmosphere, therefore impacting many other reactions. Global $CH_4$ concentrations have risen dramatically since pre-industrial times [e.g., *Intergovernmental Panel on Climate Change* (*IPCC*), 2007], but the rate of increase since 2000 has been very small [*Dlugokencky et al.*, 2003; *IPCC*, 2007]. The $CH_4$ growth rate varies from year to year, depending on factors such as wetland emission [*Dlugokencky et al.*, 2001] and biomass burning [*Butler et al.*, 2005]. Large emissions have been observed in recent years from the Siberian peatlands [*Smith et al.*, 2004] and from sources in South America [*Frankenberg et al.*, 2005, 2006; *do Carmo et al.*, 2006].

[9] $CH_4$ is measured at surface stations throughout the world, primarily at remote sites, with extremely low uncertainty (1–3 nmol/mol, or ppb) [*Dlugokencky et al.*, 2003; http://www.esrl.noaa.gov/gmd/ccgg/]. Ground-based measurements from Fourier transform infrared spectrometers (FTIRs) provide information above the boundary layer, but stations are sparse and may not be representative of large scales. Spaceborne measurements are less accurate, but can provide extensive spatial and temporal coverage that can help to better understand the variations of methane on global scales. $CH_4$ has been observed in the stratosphere and the upper tropopause region from the Halogen Occultation Experiment (HALOE) on the Upper Atmosphere Research Satellite (UARS) [*Schoeberl et al.*, 1995; *Park et al.*, 1996; *Randel et al.*, 1998]. These data have been used to study the seasonal variation of $CH_4$ near the tropopause and in the stratosphere [*Randel et al.*, 1998; *Park et al.*, 2004]. $CH_4$ has also been measured in this altitude region by the Michelson Interferometer for Passive Atmospheric Sounding (MIPAS) on Envisat [*Payan et al.*, 2007] and by the Atmospheric Chemistry Experiment (ACE) [*Nassar et al.*, 2005; *De Mazière et al.*, 2007].

[10] Nadir-viewing spaceborne measurements of tropospheric $CH_4$ include those from the Interferometric Monitor for Greenhouse Gases (IMG) from the Advanced Earth Observing Satellite (ADEOS) [*Clerbaux et al.*, 2003], the Scanning Imaging Absorption Spectrometer for Atmospheric Chartography (SCIAMACHY) on the ESA Envisat satellite [*Frankenberg et al.*, 2005, 2006] and the Atmospheric Infrared Sounder (AIRS) on the NASA Aqua satellite [*Xiong et al.*, 2008]. The Infrared Atmospheric Sounding Interferometer (IASI) on the latest METOP satellite also offers the capability of tropospheric $CH_4$ measurements [*Ravazi et al.*, 2009; *Crevoisier et al.*, 2009].

[11] The Tropospheric Emission Spectrometer (TES) on the EOS-Aura platform is a nadir-sounding infrared Fourier transform spectrometer designed to study the Earth's ozone, air quality and climate [*Beer et al.*, 2001]. TES primarily makes nadir observations of spectral radiances in the spectral range 650–3050 $cm^{-1}$ (3.3–15.4 microns) at 0.1 $cm^{-1}$ spectral resolution (apodized) in the nadir-viewing mode. Profiles of atmospheric temperature, $O_3$, $H_2O$, HDO, CO and $CH_4$ as well as cloud effective optical depths are retrieved operationally and are publicly available through the NASA Langley Atmospheric Science Data Center (ASDC). Additional species retrieved from the TES data (not currently operational) include $NH_3$ and $CH_3OH$ [*Beer et al.*, 2008]. The TES operational retrieval is a constrained nonlinear least squares fitting procedure. Further details of the retrieval method and error analysis are given by *Bowman et al.* [2006] while a description of the constraints applied is given by *Kulawik et al.* [2006b]. The TES data set considered in this analysis is Version 3 (V003).

[12] The TES $CH_4$ retrieval uses microwindows at 1292.02–1305.76 $cm^{-1}$ and 1307.02–1307.8 $cm^{-1}$. During the operational processing, the TES $CH_4$ profiles are retrieved in log(volume mixing ratio (VMR)) on 14 pressure levels and then linearly mapped to a finer 67-level grid [*Bowman et al.*, 2006]. This fine grid is the one on which the forward model and Jacobian calculations are performed [*Clough et al.*, 2006]. All TES nadir Level 2 trace gas products are supplied on this 67 level grid. (From here on, "forward model grid" will refer to the 67 levels and "retrieval grid" will refer to the 14 levels.) The TES V003 a priori profiles were constructed from the Aura monthly climatology, based on runs from the MOZART global chemical model [*Brasseur et al.*, 1998] in blocks of 30° latitude by 60° longitude.

[13] The retrieved profile can be expressed as a first-order expansion in $(\mathbf{x} - \mathbf{x_a})$ [*Rodgers*, 2000]:

$$\hat{\mathbf{x}} = (\mathbf{I} - \mathbf{A})\mathbf{x}_a + \mathbf{A}\mathbf{x} + \varepsilon \quad (1)$$

where $\mathbf{x}_a$, $\hat{\mathbf{x}}$ and $\mathbf{x}$ are the prior, retrieved and true profile state, $\mathbf{I}$ is the identity matrix, $\mathbf{A}$ is the averaging kernel matrix, which describes the sensitivity of the retrieval to the true state, and $\varepsilon$ represents the error. The number of degrees of freedom for signal is defined as the trace of the averaging kernel matrix. When the averaging kernel matrix, $\mathbf{A}$, is unity then changes to the prior have no effect on the retrieved value. Figure 1 shows four sets of representative TES averaging kernels for $CH_4$ retrievals and the approximate vertical range over which these retrievals provide useful information. A useful diagnostic here is the sum of the row of the averaging kernels, which in general can be thought of as a rough measure of the fraction of the retrieval that comes from the data, rather than from the a priori. (Note that this is only a rough measure; in the examples presented, the sum of the row of the averaging kernels actually exceeds unity at some altitudes.) Broadly speaking, the sensitivity of the TES $CH_4$ retrievals peaks between 200 and 400 hPa. Over hot surfaces, such as the desert example shown in Figure 1b, TES may show greater sensitivity close to the surface, but this is not the case over most of the globe. The upper altitude bound of the sensitivity of TES $CH_4$ retrievals generally follows the tropopause.

[14] The sensitivity of the TES $CH_4$ retrievals is further demonstrated in Figure 2, which shows the degrees of freedom for signal for the TES $CH_4$ retrievals for all measurements for January, April, July and October 2006 that pass certain quality checks. The quality controls applied here were those suggested in the TES Level 2 User's Guide [*Osterman et al.*, 2008], apart from the check on retrieved

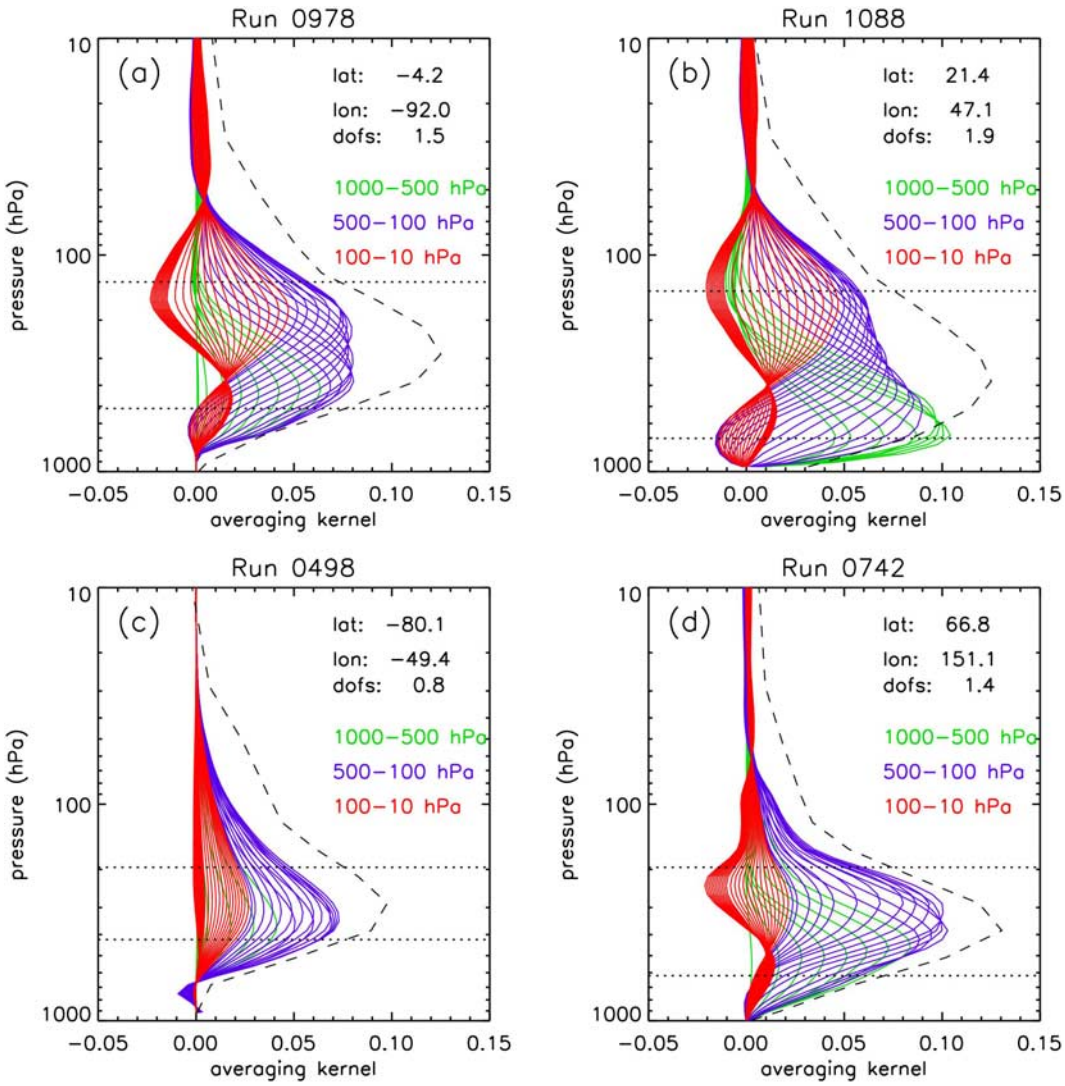


**Figure 1.** Solid lines show example averaging kernels (on the TES forward model levels) for four cases from one global survey from July 2006: (a) tropical profile over ocean, near Galapagos islands; (b) low latitude over desert surface; (c) high latitude over Antarctica (polar winter); and (d) high latitude over Siberia (polar summer). The latitude, longitude, and degrees of freedom for signal (DOFS) for each of these TES sequences is shown on the plots. The dashed profile shows the sum of the row of the averaging kernel at each pressure level, scaled by a factor of 0.1. The dotted horizontal lines show the pressure levels at which the sum of the row of the averaging kernel drops below 0.7, providing a guide to the approximate vertical range over which the TES retrieval provides useful information.

average cloud effective optical depth. The User's Guide suggests a threshold optical depth of 10.0, but here all measurements with an average cloud effective optical depth greater than 1.0 have been neglected. (Further information on the TES cloud optical depth retrievals is given by *Osterman et al.* [2008] and *Kulawik et al.* [2006a].) The cloud optical depth threshold of 1.0 was chosen as a compromise between a threshold low enough that the impact of cloud on the measured radiances would be minimal and a threshold high enough not to screen out measurements to the point of adversely affecting global coverage. It can be seen from the maps in Figure 2 that the degrees of freedom for signal for the TES $CH_4$ retrievals are strongly correlated with surface temperatures, showing the highest values over hot, desert surfaces and the lowest values over surfaces in polar winter in both hemispheres. Values range from almost 2.0 to 0.5. It can also be seen that there is some correlation between degrees of freedom for signal and tropopause height. This is expected for $CH_4$, which is well mixed in the troposphere and falls off rapidly with altitude in the stratosphere.

[15] Since the TES Level 2 data are supplied on a 67-level grid, the initial reaction of potential data users might be to look at the data in terms of, say, global maps on a given pressure level. This would be an obvious approach to certain types of analysis of output from a global chemical model. However, given that the total number of degrees of freedom for signal for each retrieved profile lies somewhere between 0.5 and 2.0, it is readily apparent that choosing to view the data on only one of the 67 TES forward model

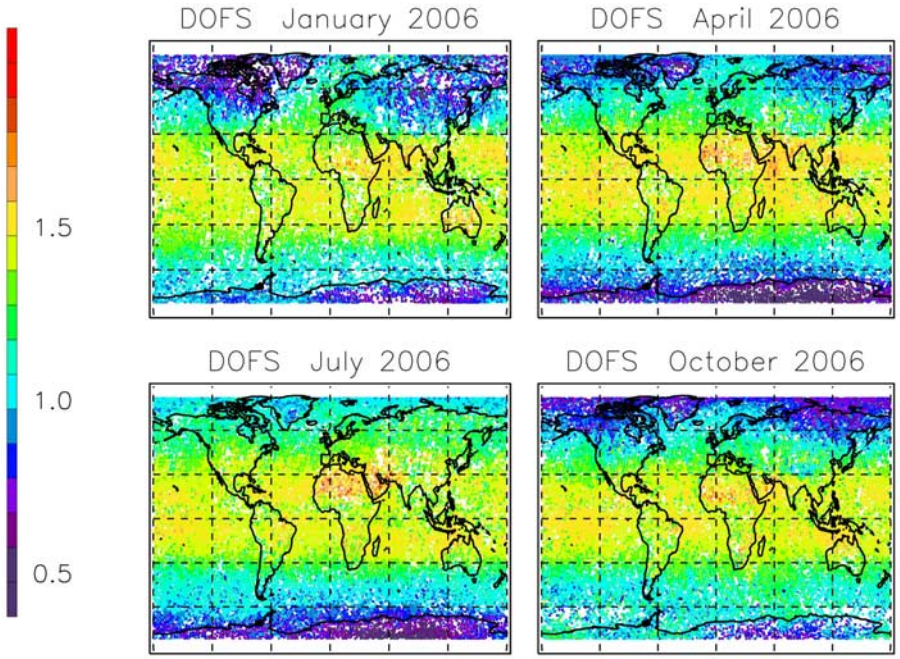


**Figure 2.** Maps of the degrees of freedom for signal for TES $CH_4$ for January, April, July, and October 2006.

levels is far from ideal. Figure 3 shows maps of $CH_4$ VMR from the 348 hPa pressure level, from the TES Level 2 files from the ASDC for four months from 2006. This pressure level was chosen because the TES retrieval is expected to have its best sensitivity here at all latitudes. Also shown on Figure 3 are the latitudes where there are changes in the TES a priori constraint vector and constraint matrix. A discontinuity in the VMR values is apparent at 30°N, which is one of the locations where there is a change in the a priori state vector. (No discontinuities are observed at locations where the constraint matrix changes.) This is particularly obvious in the July data, but is also visible in other months. It is clear from Figure 3 that the values at any one given pressure level (of the 67 supplied) are strongly sensitive to

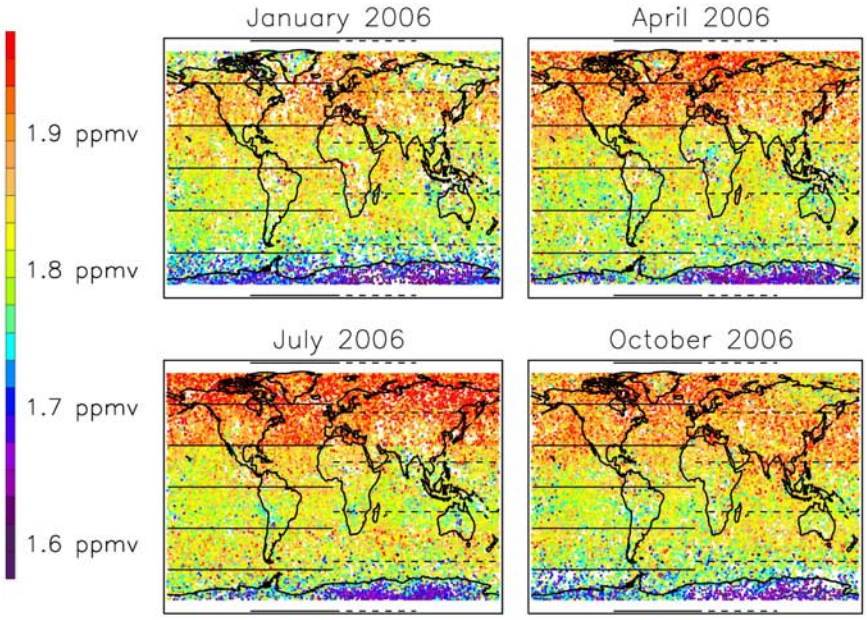


**Figure 3.** Maps of VMR at 348 hPa from TES Level 2 product from January, April, July, and October 2006. Solid horizontal lines show the boundaries of the different latitude bins for the constraint vector ($x_a$), every 30° latitude. Dashed horizontal lines show the boundaries of the different constraint matrices used (18°N/S, 54°N/S).

the a priori profile used. It is apparent that an analysis of latitudinal gradients, which are extremely small for $CH_4$, would not be possible here and that temporal changes in the a priori would also severely limit the usefulness of analyses of time series. Aside from these issues, global maps of this product on a particular pressure level are somewhat misleading for two reasons. First, the vertical resolution is coarse: the width of the averaging kernel for any given reported level is several kilometers wide. Second, the level at which the measurement is most sensitive varies somewhat with geographical location, according to surface temperature, surface elevation, atmospheric temperature, trace gas concentration and distribution of clouds.

[16] The intention in this study is to use the TES Level 2 $CH_4$ as an example of a product where the representation may be changed in order to reduce the a priori influence and so facilitate the scientific interpretation of the data. Some examples of scientific interpretation of the TES $CH_4$ data will be presented in order to demonstrate the utility of the approach, but the overall aim is to present a methodology that may be applied to similar data products from this or other satellite instruments. The technique presented in this work could be considered a TES Level 3 $CH_4$ product that would be of use to the community. The model comparisons presented may be regarded as an interesting piece of the large-scale validation of the TES $CH_4$ product, which is currently underway. However, the primary focus of this paper is intended to be the representation of the data.

## 3. Representative Tropospheric Volume Mixing Ratio

[17] The aim of the approach presented here is to move to a representation in which the number of elements in the state vector is more representative of the number of independent pieces of information in the measurement (DOFS), and where the influence of the a priori data on the final product is reduced. In order to eliminate the a priori influence, it is necessary to move to a representation in which the diagonal of the averaging kernel is unity. For the example data set of TES $CH_4$ used here, the DOFS for the retrieval is less than 1.0 over large regions of the globe, with other larger regions where DOFS is much large than 1.0 but less than 2.0.

[18] The approach adopted here is simply a linear transformation from a finer to a coarser grid. The change in representation from the finer set of forward model levels, $\mathbf{p_f}$, to the coarser subset of retrieval levels, $\mathbf{p_c}$, is accomplished by means of a linear mapping using the transformation matrix

$$\mathbf{W}^* = \left(\mathbf{W}^\mathbf{T}\mathbf{W}\right)^{-1}\mathbf{W}^\mathbf{T} \tag{2}$$

where $\mathbf{W}$ is the interpolation matrix which samples the coarse grid profile vector on the fine grid [*Rodgers*, 2000; *von Clarmann and Grabowski*, 2007]. The state vector on the coarse grid, $\mathbf{x_c}$, is then

$$\hat{\mathbf{x}}_c = \mathbf{W}^*\hat{\mathbf{x}}_\mathbf{f} \tag{3}$$

(where $\mathbf{x_f}$ is the state vector on the fine grid) and the averaging kernel on the retrieval grid is

$$\mathbf{A}_c = \mathbf{W}^*\mathbf{A_f}\mathbf{W}. \tag{4}$$

The retrieval error covariance on the retrieval grid is

$$\hat{\mathbf{S}}_\mathbf{c} = \mathbf{W}^*\hat{\mathbf{S}}_\mathbf{f}\mathbf{W}^{*\mathbf{T}}. \tag{5}$$

Note that no information is lost in the transformation from the forward model level grid supplied in the TES level 2 product files to the retrieval level grid, since the retrieval levels were actually mapped to the forward model levels using the matrix $\mathbf{W}$ in the creation of the TES product files. However, any subsequent transformation to a coarser grid than the retrieval grid must result in some kind of information loss.

[19] The move to the coarse grid raises two questions: how many levels should be in the new grid and where should they be? *Von Clarmann and Grabowski* [2007], working with limb-sounding retrievals, proposed a mapping matrix with levels determined by summing the diagonal of the averaging kernel from the bottom level up. The number of levels is determined by the total integer number of DOFS and the new, coarse grid has levels at points where the sum reaches an integer number of DOFS. The characteristics of averaging kernels for limb-sounding retrievals are fundamentally different to those of nadir retrievals. Limb-sounding averaging kernels are in general relatively narrow and sharply peaked, peaking at the retrieval pressure/altitude to which they are attributed. For nadir sounders the averaging kernels are typically very broad. The signal measured by the nadir instrument represents a wide altitude range and the averaging kernel for a given retrieval level may not necessarily peak at the level to which it has been ascribed. In some cases, nadir averaging kernels may be doubly peaked. For the nadir data considered here, there are cases where an integer number of DOFS are not reached over the whole profile. For this reason, a different approach to define the new, coarse grid has been adopted here. Consider the Galapagos case with averaging kernels as shown in Figure 1a, with a total number of DOFS of 1.48. Figure 4 shows the cumulative trace of the averaging kernel for this case. For this example, it is apparent that the incremental increase in the DOFS with altitude is small above the 110 hPa retrieval level. At this level, the cumulative trace of the averaging kernel is 1.28, which is basically the DOFS for the troposphere in this retrieval. This number is somewhat greater than 1.0, indicating that there is some information on the vertical structure of the tropospheric profile, but less than 2.0, indicating that an attempt to present more than one representative number for the troposphere will yield quantities that are not independent.

[20] Figure 5 shows a possible transformation of the averaging kernel (see equation (4)). Figure 5a shows the averaging kernel on the retrieval levels. It is clear from the width of the averaging kernel functions and their overlap that the tropospheric levels in the corresponding state vector are strongly interdependent and that the value of the diagonal of the averaging kernel matrix at any given level is exceedingly small. It is also evident from the sum of the

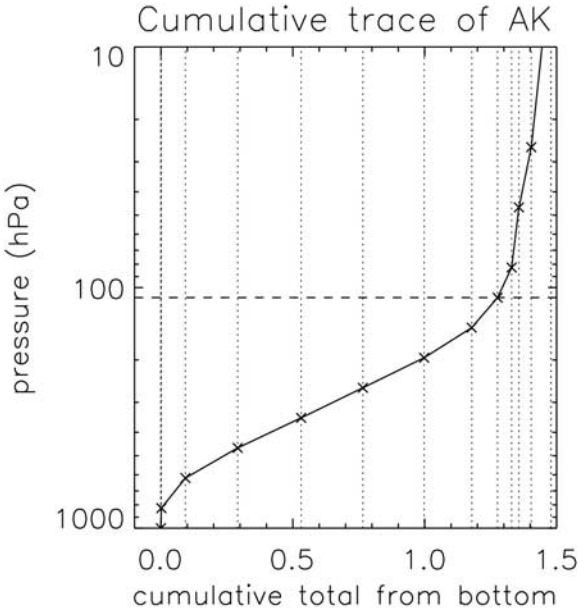


**Figure 4.** Cumulative trace of the $CH_4$ averaging kernel matrix from TES run 4519, sequence 2827 (see also Figure 1a), on the fourteen-level pressure grid used in the retrieval.

row of the averaging kernels that the retrieved values in the lower troposphere and in most of the stratosphere are entirely dominated by the a priori constraint vector. Figure 5b shows the averaging kernel for a transformation that results in only one element of the state vector in the troposphere, where the averaging kernel function approaches unity. This scenario provides a reduction of a priori influence, but now loses any attempt to characterize vertical structure in the troposphere. The coarse grid here consists of a subset of four of the retrieval levels: one at the surface, one in the troposphere, one just above the troposphere, at the point where the information in the TES retrieval drops off and one at the top of the atmosphere. Grid points other than the tropospheric points may be considered merely as anchor points. Although there are four points in the new coarse grid, the tropospheric "level" is now the only one that contains any information of interest The end product is now one number that represents tropospheric methane, and the result should no longer be thought of as a profile. Neither should this number be thought of as a tropospheric column, since the sensitivity of the TES instrument to methane is in the middle to upper troposphere and not the boundary layer where most of the molecules in the atmosphere lie. The number is not really a partial column either. Rather, it is a "representative tropospheric VMR" (RTVMR), a value that represents the mixing ratio in the middle to upper troposphere, where the instrument is most sensitive to methane. The location of the tropospheric pressure level in Figure 5 was chosen to be at the retrieval level below where the value of the sum of the row of the averaging kernel was at a maximum, in order to best reflect the sensitivity of the measurement. The closest retrieval level to the peak of the sum of the row of the averaging kernels is at 348 hPa for this case. The level below this was chosen in order to weight the transformation for this wide layer lower in the atmosphere, where there are more methane molecules. The width of the transformed averaging kernel spans the troposphere. This representation results in a loss of a fractional number of degrees of freedom, but offers the advantage of significantly reduced a priori influence.

[21] As pointed out by *von Clarmann and Grabowski* [2007], a simple transformation to a coarse grid, as performed here, does not prevent the resulting averaging kernels from overlapping. While most of the overlaps of the original averaging kernels fall within the altitude region represented by the "tropospheric" grid point, there is still something of a "border effect" present. The result here is somewhat sensitive to the choice of the tropopause anchor point since there is a fractional number of degrees of

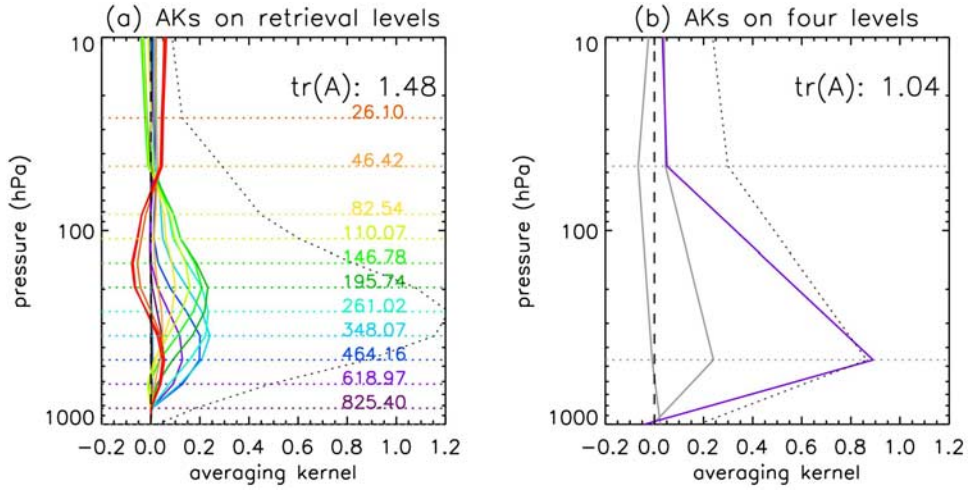


**Figure 5.** Example averaging kernels for the case shown in Figure 1a. (a) The fourteen levels used in the TES $CH_4$ retrieval. Colors show pressures assigned to each row of the averaging kernel, demonstrating that the retrieval information for a given labeled pressure level may not originate at that pressure. The black dotted line shows the profile of the sum of the rows of the averaging kernel. (b) With only one level in the troposphere. The purple line shows the tropospheric averaging kernel.

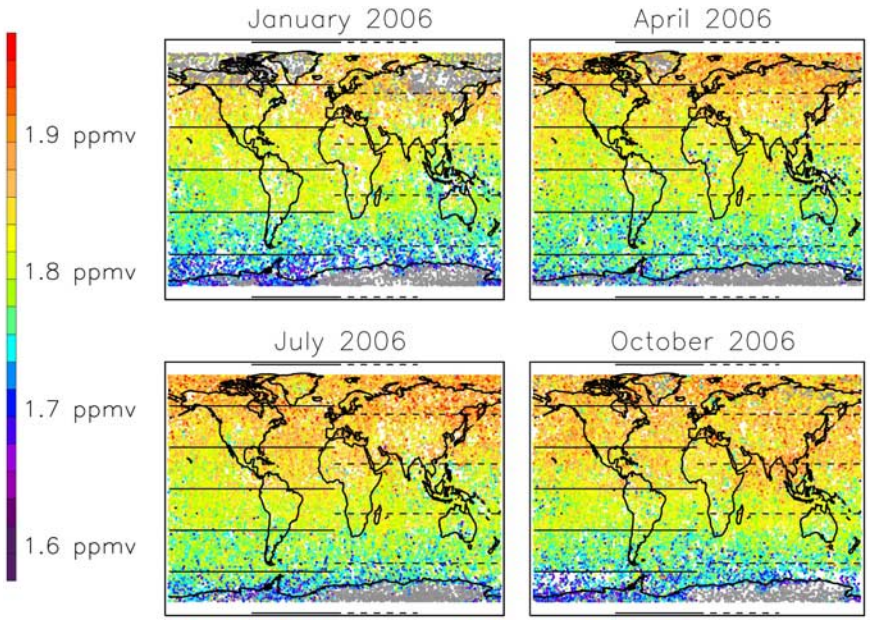


**Figure 6.** Representative tropospheric VMR (RTVMR) for TES methane for January, April, July, and October 2006. Gray points show measurements where the sum of the row of the averaging kernel did not have a value greater than 0.7 for any point in the Level 2 profile.

freedom in the retrieval that is not associated with the tropospheric point. If the tropopause anchor point is placed too low in altitude, then there is some division of information between the tropospheric point and the tropopause point. However, if the tropopause anchor point is placed too high in altitude, there is a larger contribution of information from the stratosphere to the tropospheric point. The tropopause anchor point was placed at the retrieval level where the sum of the row of the averaging kernels falls below 0.4. For an analysis of $CH_4$ profiles over a range of conditions, this seems to provide the optimum placing of coarse grid points, maximizing the information for the tropospheric point for this particular set of atmospheric conditions, while minimizing stratospheric influence. Note that the grid shown in Figure 5 is applicable to this specific case. In the application of this approach to a global data set, a simple algorithm was applied to determine a coarse grid for each individual case. The steps in the algorithm to determine the coarse grid were as follows: (1) determine the retrieval level at which the sum of the row of the averaging kernels is at a maximum and take the next lower retrieval level to be the tropospheric level, (2) determine the retrieval level at which the sum of the row of the averaging kernel drops below 0.4 and take this to be the "tropopause" level, and (3) set the uppermost and lowermost retrieval levels as anchor points. Note that the transformation to the coarse grid may be performed with either the 67 forward model levels or the 14 retrieval levels as a starting point, as long as the coarse grid levels are always chosen to be a subset of the 14 retrieval levels.

[22] We acknowledge that other techniques may be more appropriate when there are more degrees of freedom available, or when the goal is to get as much information as possible about a predetermined level in the atmosphere. One reason why this approach is particularly applicable to $CH_4$ is that most of the overlaps of the original averaging kernels fall within the altitude region represented by the "tropospheric" grid point. For species with larger number of degrees of freedom available, the issue of overlap would need to be carefully considered. Also, the application of the approach presented here would be problematic for species such as ozone that have a strong stratospheric contribution to the tropospheric averaging kernels. We also recognize that some users may prefer to work in eigenvector, rather than geophysical, space.

[23] Other satellite teams have chosen different ways to represent $CH_4$ retrievals. IMG [*Clerbaux et al.*, 2003] methane values are reported as a total column only. The SCIAMACHY level 2 methane product is reported in terms of vertical column densities for three atmospheric layers, where only the lowest layer contains significant information [*Frankenberg et al.*, 2005]. The SCIAMACHY team has chosen to report a column-averaged VMR which is representative of the altitude range where the instrument is sensitive. The AIRS retrieval approach for $CH_4$ is described by *Susskind et al.* [2003] and by *Xiong et al.* [2008]. For the AIRS product, profiles are reported in terms of seven layers. Xiong et al. state that the most sensitive layer in the tropics is about 200–300 hPa, decreasing in altitude to 400–500 hPa near the poles.

## 4. Results and Interpretation

### 4.1. RTVMRs From TES

[24] The transformation described in the previous section was applied to the TES $CH_4$ retrievals for four months in 2006. The results are shown in Figure 6. The discontinuities in VMR values observed at 30°N due to the change in the a priori constraint vector in the 348 hPa level maps in Figure 3 are not seen in this new representation. The RTVMR shown in Figure 6 represents a single value for the troposphere, representing information coming from the measurement.

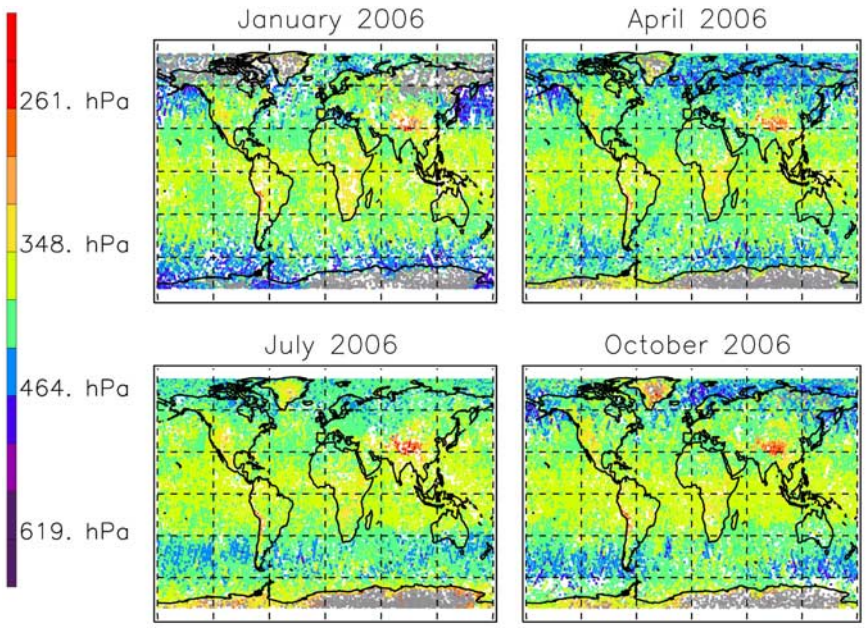


**Figure 7.** Maps of "effective pressure" for the TES $CH_4$ RTVMR for January, April, July, and October 2006. Gray points show measurements where the sum of the row of the averaging kernel did not have a value greater than 0.7 for any point in the Level 2 profile.

[25] In order to aid the interpretation of this RTVMR, Figure 7 shows maps of an "effective pressure" for this quantity, where the effective pressure is defined below:

$$\bar{p} = \frac{\sum_{i=1,67} a_i n_i p_i}{\sum_{i=1,67} a_i n_i}. \quad (6)$$

Here, **n** is the vector of the number density of air, supplied on 67 forward model levels in the TES Level 2 files (where $n_i$ is the *i*th forward model level), **p** is the vector of pressure on the forward model levels and **a** is the row of the transformed averaging kernel, $\mathbf{A_c}$, that corresponds to the troposphere, interpolated onto the fine grid of 67 forward model levels. The weighting by number density is included in the calculation of the effective pressure in order to account for the fact that a wide atmospheric layer (i.e., the

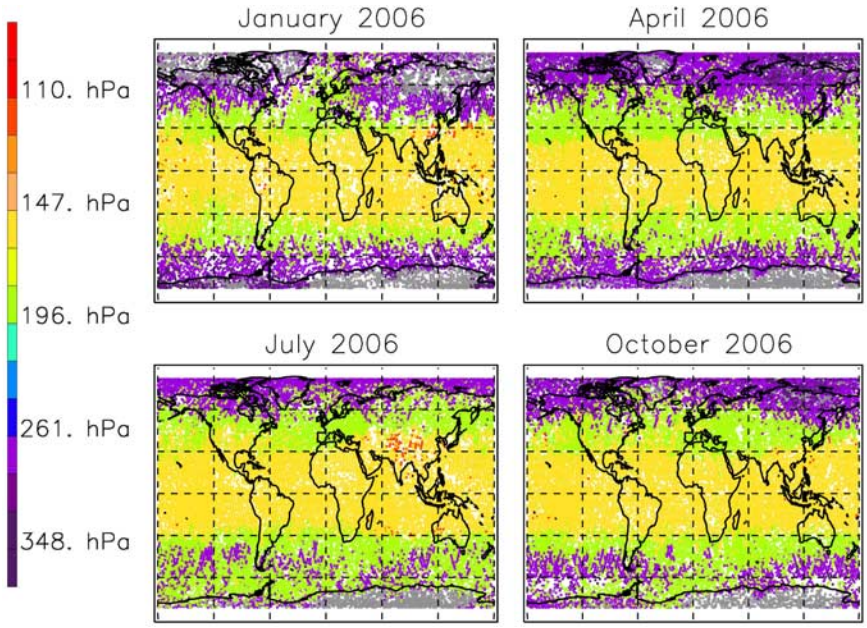


**Figure 8.** Upper bound pressure for the RTVMR fields shown in Figure 6. The upper bound pressure was defined as the pressure for which the sum of the row of the averaging kernels drops below 0.7. Gray points show measurements where the sum of the row of the averaging kernel did not have a value greater than 0.7 for any point in the Level 2 profile.

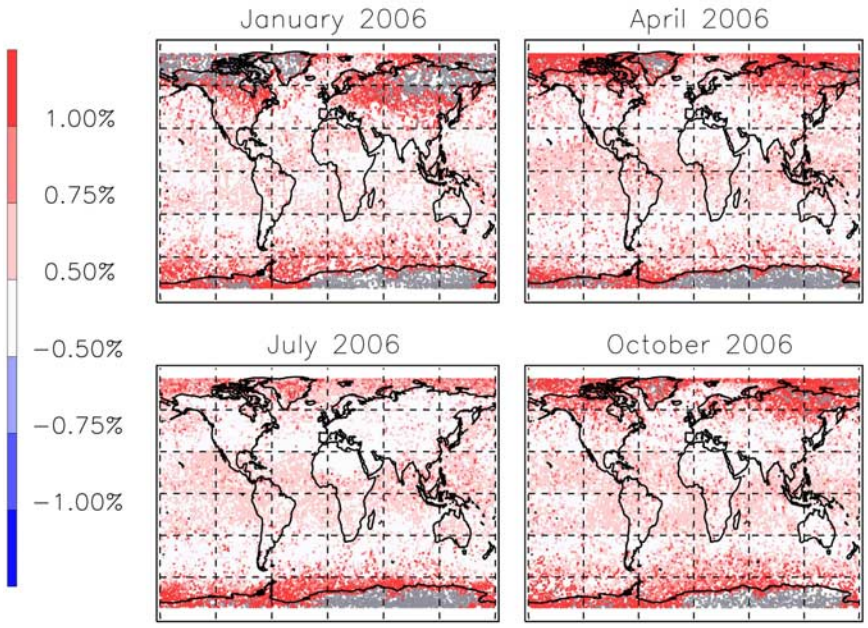


**Figure 9.** Differences in TES $CH_4$ RTVMR induced by a uniform increase of 5% in the a priori constraint vector.

whole troposphere) is being represented, and that there is a significant gradient in the number density from the bottom to the top of the layer. The effective pressure reflects where most of the information in the RTVMR comes from. It can be seen from Figure 7 that the effective pressure is influenced by topography. It is lower over regions where the surface is at high altitude, such as the Tibetan Plateau or the Andes. This correlation with topography is not observed in the DOFS for the retrieval (see Figure 2). Some land-sea contrast is also apparent, particularly in the northern hemisphere in winter (January). Figure 8 shows maps of an approximate upper bound for the sensitivity of the TES retrieval, defined here as the retrieval level at which the sum of the row of the averaging kernels drops below 0.7. Note that if the retrieval had not previously been performed on a finer grid, it would not be possible to characterize the sensitivity of the measurement in this way. (A quantitative discussion of the detrimental effect of ignoring the effective pressure is provided in the next section.)

[26] In order to effectively eliminate the influence of the a priori, the diagonal element of the averaging kernel for the RTVMR should be unity. In geographical regions where the DOFS for the TES retrieval is greater than one (see Figure 2), this number is indeed close to unity for the transformed RTVMR product. In regions such as Antarctica and the winter Arctic, this number is close to the value of the available number of DOFS, which may be as low as 0.5. However, even in these more problematic regions, the influence of the a priori on the RTVMR is far smaller than the influence of the a priori on any given one of the forward model levels supplied in the Level 2 data file.

[27] In order to demonstrate the remaining a priori influence on the RTVMR product, Figure 9 shows differences in the RTVMR induced by a 5% uniform increase in the a priori across the globe. Adjustment to the alternative prior was achieved using the following equation [*Rodgers and Connor*, 2003]:

$$\hat{\mathbf{x}}' = \hat{\mathbf{x}} + (\mathbf{I} - \mathbf{A})(\mathbf{x}_a' - \mathbf{x}_a) \tag{7}$$

where $\mathbf{x}_a$ and $\mathbf{x}_a'$ are the original and new priors, respectively, $\hat{\mathbf{x}}$ is the original retrieved value and $\hat{\mathbf{x}}'$ is the retrieved value with the new prior. In higher latitudes, in regions where the DOFS for the retrieval was less than one (see Figure 2), the a priori influence is still present. However, the a priori influence on the RTVMR is significantly reduced compared to a product based on one forward model level.

### 4.2. Comparison With a Global Chemical Model

[28] In order to further demonstrate the utility of the proposed approach, comparisons were performed with output from GEOS-Chem, a global chemical model. A general description of the GEOS-Chem model is given by *Bey et al.* [2001]. The $CH_4$ simulation is described by *Wang et al.* [2004], and evaluated with measurements from ground-based stations and aircraft profiles in that study and in the study by *Xiao et al.* [2004]. The $CH_4$ fields used in these comparisons were generated using 2001 meteorology by *Xiao et al.* [2004].

[29] Although the TES data and the model data are not from the same year, globally averaged $CH_4$ has not grown over the given period [*IPCC*, 2007; E. J. Dlugokencky et al., Atmospheric methane dry air mole fractions from the NOAA ESRL Carbon Cycle Cooperative Global Air Sampling Network, 1983–2006, Version: 2007-09-19, 2007, available at ftp://ftp.cmdl.noaa.gov/ccg/ch4/flask/event/]. Figure 10 shows surface measurements from the NOAA Earth System Research Laboratory (ESRL) Global Monitoring Division (GMD) Carbon Cycle Cooperative

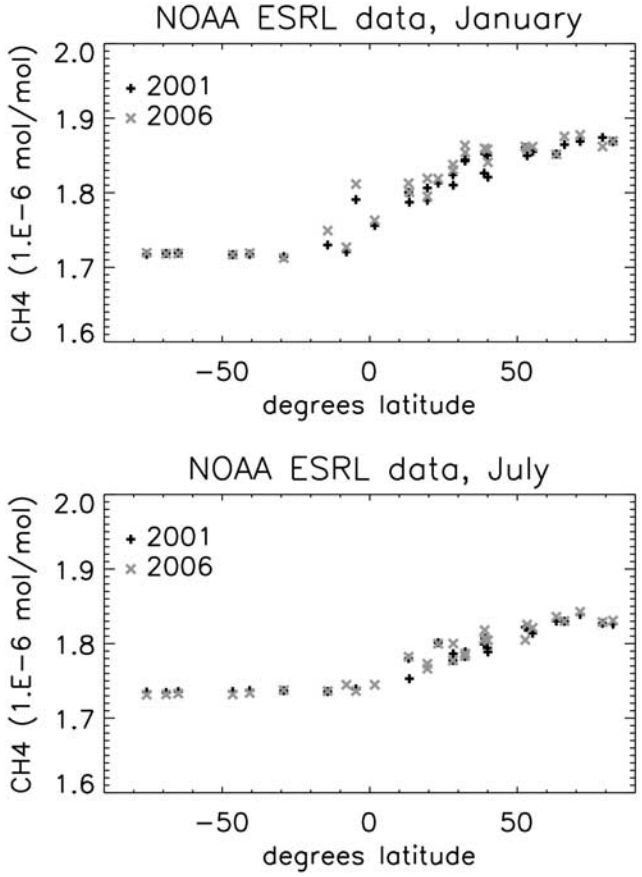


**Figure 10.** NOAA ESRL remote station surface monthly mean surface measurements for January and July, showing the similarity between the 2001 and 2006 values.

Global Air Sampling Network (see ftp://ftp.cmdl.noaa.gov/ccg/ch4/flask/event/) from remote stations for both 2001 and 2006 plotted against latitude. Differences between the measurements from these 2 years are small.

#### 4.2.1. Latitudinal Gradients

[30] Zonal means in 10° latitude bins were calculated for both the TES RTVMRs and similarly mapped TES initial guess/a priori for January and July 2006. Zonal means were also calculated for RTVMRs from the GEOS-Chem 2001 monthly mean global fields provided by Y. Xiao (personal communication, 2007). In order to calculate the GEOS-Chem RTVMRs, the following steps were applied. For each TES profile, the ''raw'' GEOS-Chem profile from the corresponding latitude/longitude grid point was interpolated onto the TES 67-level forward model grid. The TES a priori constraint vector and averaging kernels were then applied to the interpolated GEOS-Chem profile, using equation (1) (where the interpolated GEOS-Chem profile is assumed to be the ''true'' state, x) to produce a ''GEOS-Chem retrieved state.'' This GEOS-Chem retrieved state was then mapped onto the same coarse grid as the TES RTVMR in order to produce a GEOS-Chem RTVMR. Theses GEOS-Chem RTVMRs represent what the TES instrument would have measured if GEOS-Chem were a true representation of the atmospheric state.

[31] An ''unbiased'' GEOS-Chem RTVMR may also be calculated without the application of the TES prior. Such a quantity takes into account the vertical resolution of the TES measurement, but is not biased by the values or shape of the TES a priori constraint vector. To calculate these ''unbiased'' GEOS-Chem RTVMRs, the GEOS-Chem profiles from the corresponding latitude/longitude grid points were interpolated onto the TES 67-level forward model grid, and then these interpolated profiles were mapped directly (using equation (3)) onto the coarse grid used to calculate the TES RTVMR for each measurement point.

[32] Results are shown in Figure 11. Figures 11a and 11b show the absolute values of the zonal mean RTVMRs with their standard deviations in Figures 11c and 11d. The TES zonal means exhibit a general high bias with respect to the GEOS-Chem values. To highlight latitudinal gradients, Figures 11e and 11f show the same zonal means, with bias removal, where the zonal mean values of the TES RTVMR and TES a priori have been scaled using the ratio to the GEOS-Chem fields (with TES a priori applied) in the 50–60°S bin. The air in this location is not affected by local emissions, and the retrievals in this region should not be affected by problems associated with retrievals over the cold, icy Antarctic surface. (The GEOS-Chem RTVMR with TES a priori applied was chosen as the reference because it has smaller latitudinal gradients than TES or the prior, and because we wish to easily compare the TES RTVMRs with the values that would have resulted from a TES measurement if GEOS-Chem was ''truth.'') It is apparent that the latitudinal gradient in the prior is far greater than the gradients observed in either the TES retrievals or in the GEOS-Chem fields. The gradient of the TES RTVMR is essentially the same as GEOS-Chem in January, but is larger than that of the model in July. The differences between the TES and GEOS-Chem RTVMRs in Figures 11e and 11f are within the standard deviations of the TES zonal means, but are of the order of 50 times larger than the standard error on the zonal means (where the standard error is the standard deviation divided by the square root of the sample size), indicating that the differences in TES and GEOS-Chem July latitudinal gradients are significant. Also shown in Figures 11g and 11h are zonal means of the ''fraction of explained variance'' (FEV), the diagonal element of the averaging kernel for the RTVMR. It can be seen that the zonal means for the diagonal element of the averaging kernels are close to 1.0 over most over the globe. Values are smaller toward the poles, especially for polar winter, where cold atmospheric and surface temperatures limit the degrees of freedom for signal available for the TES retrieval.

[33] Figure 11 represents latitudinal gradients in the middle to upper troposphere. In order to examine whether this has any correlation with the situation at the surface, Figure 12 compares NOAA ESRL monthly mean measurements to surface values from ''raw'' GEOS-Chem and from the TES a priori (sampled at the NOAA ESRL station locations). Surface latitudinal gradients in GEOS-Chem agree well with those of the measurements, while surface latitudinal gradients in the MOZART climatology used in the TES a priori are too large. Since GEOS-Chem provides a better representation of surface latitudinal gradients than the TES a priori (MOZART Aura climatology), it might also be expected that the GEOS-Chem latitudinal gradients in the mid to upper troposphere are more representative of the

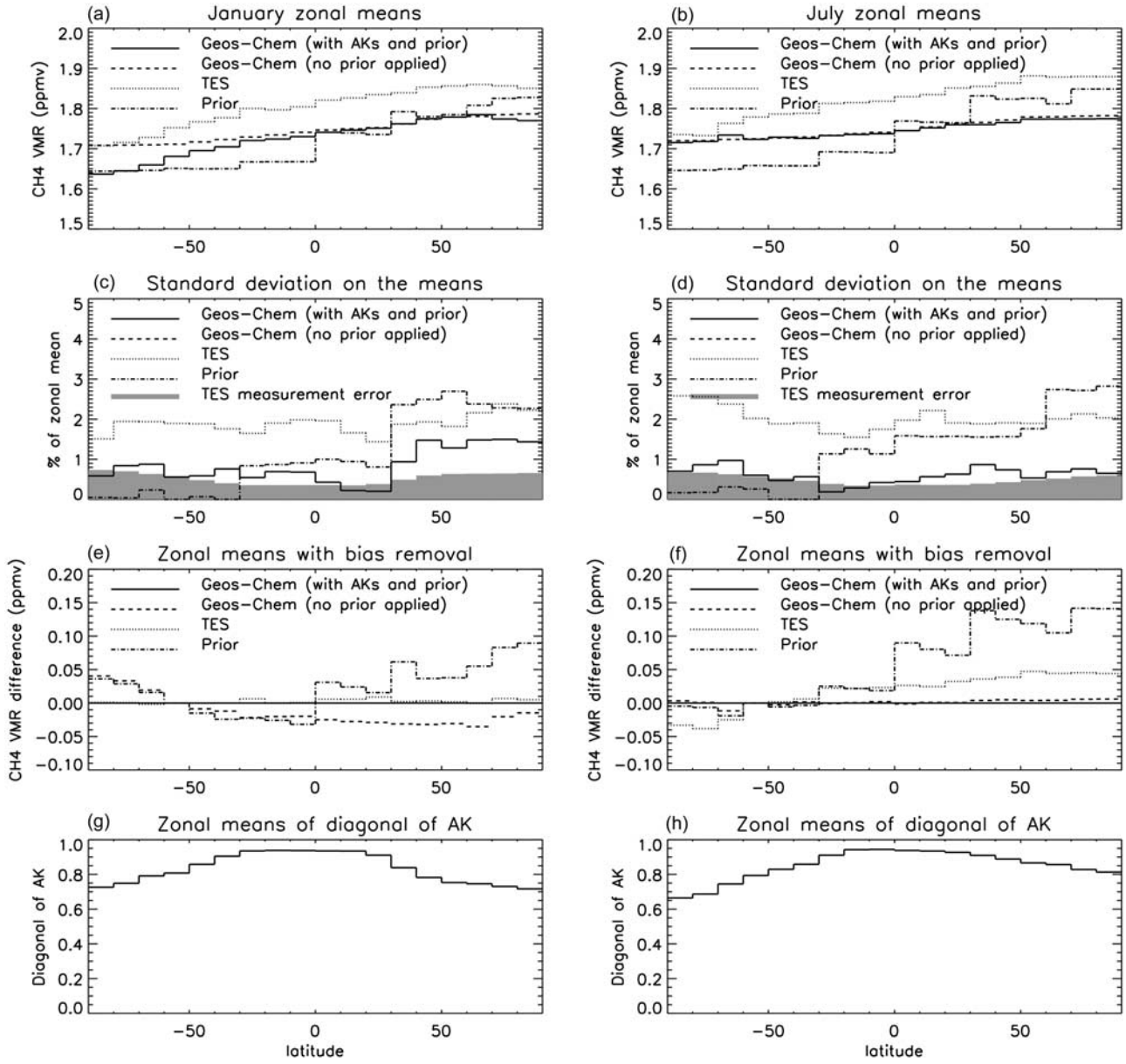


**Figure 11.** (a and b) Zonal means of RTVMR for January and July calculated using 10° latitude bins from TES, GEOS-Chem with TES averaging kernels and a priori applied, GEOS-Chem without the TES a priori applied, and the TES prior. (c and d) Standard deviations on these zonal means, shown with zonal means of TES measurement (random) error. (e and f) Differences of zonal means from GEOS-Chem, with bias removal based on the zonal means at 50–60°S. (g and h) Zonal mean values of the diagonal of the tropospheric averaging kernel.

true atmosphere. Therefore the fact that the TES RTVMR latitudinal gradients agree better with GEOS-Chem than with the TES prior lends confidence in the TES $CH_4$ data. Note that this analysis would not be possible using the TES $CH_4$ product on the 67 level grid.

[34] The results of this comparison should not be assumed to reflect badly on the MOZART model in general. The MOZART fields used to generate the Aura climatology date from before the Aura launch and are therefore rather old. They provide some estimate of global $CH_4$ fields and variability, but the GEOS-Chem fields were produced from a more recent and more carefully targeted study of methane and have been subject to validation in the middle to upper troposphere using data from aircraft campaigns as well as validation at the surface [*Wang et al.*, 2004; *Xiao et al.*, 2004].

#### 4.2.2. Global Distributions

[35] TES RTVMR values exhibit an overall high bias compared to GEOS-Chem, so a constant bias of 3.5% was removed from the TES values before comparing global distributions. The plots in Figure 13 show differences after the removal of a constant bias of 3.5%. This bias is the

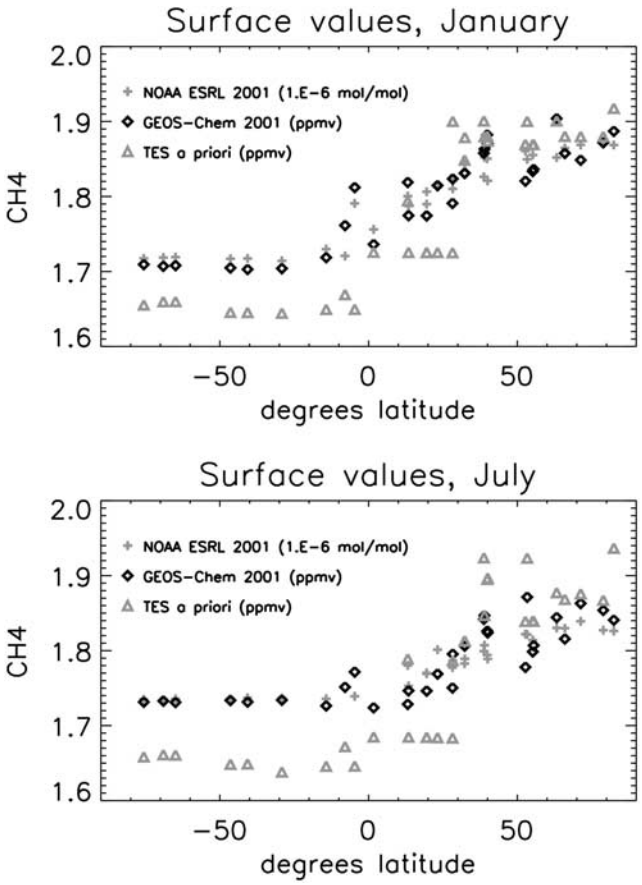


**Figure 12.** NOAA ESRL monthly mean measurements alongside surface values from GEOS-Chem and the TES a priori surface values. Surface latitudinal gradients in GEOS-Chem are in good agreement with the latitudinal gradients in the measurement, while surface latitudinal gradients in the MOZART runs used for the TES a priori are obviously too large.

difference between TES and GEOS-Chem in January at 50–60°S. Figure 13 shows percentage differences between the RTVMR calculated from the TES V003 2006 data and from the GEOS-Chem monthly mean fields for 2001. Even though the values at remote surface stations are similar for both years, it might be expected that spatial features in global maps of methane could be different, because of differences in emissions, chemistry and meteorology (transport) for the 2 years. Therefore further work would be needed in order to draw definitive conclusions about the causes of origin of the differences shown. However, some clear spatial features can be discerned with confidence in the differences between model and measurement. For example, TES RTVMRs are consistently high compared to GEOS-Chem over the tropical Atlantic. Note that this result is robust with respect to the use of cloud optical depth thresholds as low as 0.05 and so is not related to systematic errors due to clouds. High values of $CH_4$ over tropical forests were reported from SCIAMACHY observations by *Frankenberg et al.* [2005], but the emissions estimates derived from these data have now been revised in view of a high bias that was discovered in the SCIAMACHY methane due to uncertainties in spectroscopy in the SCIAMACHY spectral range [*Frankenberg et al.*, 2008a, 2008b], so a tropical forest emission explanation can probably be discounted. (It should also be noted that the SCIAMACHY measurements were primarily over land, and are sensitive closer to the surface than TES.) There could be some contribution in the region of the tropical Atlantic from South American and African biomass burning, especially during July. However, it is seems likely that the TES/GEOS-Chem differences in this region are due either to differences in 2001/2006 transport, or to retrieval artifacts, perhaps from Saharan dust. Further work would be necessary to determine the cause. Another example of an interesting spatial feature is the high $CH_4$ values observed over Indonesia in October 2006 compared to the GEOS-Chem fields for 2001. The TES $CH_4$ fields in October 2005 (not shown) do not show these high values over Indonesia. Further work would be required in order to definitively attribute the cause of the observed elevated CH4 in this region, but it is likely that the high values are related to increased biomass burning associated with the 2006 El Nino [*Logan et al.*, 2008]. Comparisons between TES and "unbiased" GEOS-Chem RTVMRs were also performed for a scenario where we did not apply the TES averaging kernels to the GEOS-Chem fields. In the RTVMR representation, the results of this comparison look very similar to the comparisons shown in Figure 13 over most of the globe. The exceptions are those regions (such as the Antarctic in summer) where the information in the TES measurement approaches the threshold for rejection. We have not attempted to draw any conclusions about these regions. Regions where the "unbiased" GEOS-Chem RTVMRs differed from the nominal results by more than 0.9% (half a division on the color scale in Figure 13) have been blocked out with gray boxes.

#### 4.2.3. Importance of the Effective Pressure

[36] In the TES/GEOS-Chem comparisons of latitudinal gradients and global distributions presented above, the vertical sensitivity of the TES measurements has been factored into the comparisons by calculating RTVMRs for the model fields. Therefore the differences in Figure 11 and Figure 13 already account for geographical and temporal variations in vertical sensitivity.

[37] As a separate consideration, the GEOS-Chem fields also provide the opportunity to quantitatively demonstrate the importance of taking the effective pressure into account when considering the TES RTVMR maps (Figure 6) alone. For example, the 50–60°N latitude band exhibits relatively large variations in effective pressure compared to other latitudes. In April (as in other months), the effective pressures in this region vary from between around 600 to 350 hPa. 390 hPa is a reasonable representative value. Assuming that the GEOS-Chem fields provide a realistic representation of the vertical variations in methane, a comparison of the GEOS-Chem values at the 390 hPa level against the "unbiased" GEOS-Chem RTVMRs provides the magnitude of the effect of vertical variations in methane values corresponding to the variation in the vertical sensitivity that is intrinsic to the TES measurement. Differences between the level mixing ratio values and "unbiased" RTVMRs for the 50–60°N latitude band in April are in general less than 2%, but may be as high as 4% in regions

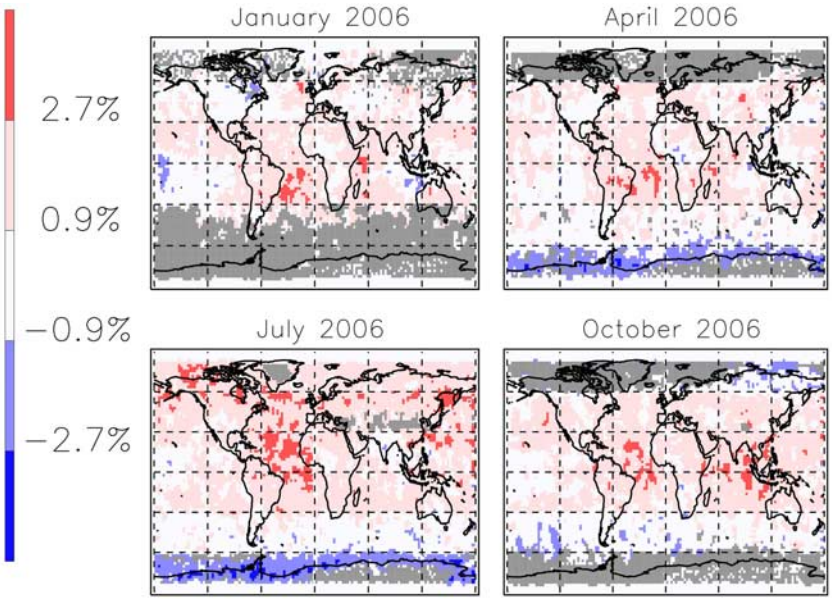


**Figure 13.** Comparisons of RTVMR from TES V003 from 2006 with RTVMR calculated from GEOS-Chem fields from 2001. (Note that the TES prior and averaging kernels were applied to the GEOS-Chem fields before the calculation of GEOS-Chem RTVMRs.) Plots show fractional differences ((TES-GC)/GC) after the removal of a constant bias of 3.5% and smoothing of difference fields using a boxcar 2 × 2 latitude/longitude boxes wide. Regions where the "unbiased" GEOS-Chem RTVMRs differed from the nominal results by more than 0.9% (half a division on the color scale in Figure 13) have been blocked out with gray boxes.

where the effective pressure deviates farthest from 390 hPa. Note that these differences are greatest for northern high latitudes and are far less significant in the tropics, where the effective pressure is more uniform. Nonetheless, these deviations are significant in the context of global variations of midtropospheric $CH_4$ and demonstrate the importance of consideration of effective pressure in the interpretation of RTVMR results.

## 5. Summary

[38] The approach presented here provides a representation of remotely sensed trace gas products where the influence of the a priori data used in the retrieval is greatly reduced. The approach uses the diagnostic information offered by the averaging kernels from retrievals on a fine grid to obtain a product that represents the sensitivity of the measurement to the atmosphere while keeping the influence of the a priori small. This type of representation can help with scientific analysis of nadir-sounding data where the number of DOFS is low, and can help to avoid misinterpretation of such data. The technique adopted in this paper is of particular use for data sets from thermal infrared instruments, where the information in the measurement does not come from the atmosphere near the surface. The approach can easily be applied to other measurements or to model output for the purposes of comparisons. The example presented here was application of the technique to the TES V003 $CH_4$ Level 2 product. The TES V003 $CH_4$ profiles contain 0.5 to 2.0 degrees of freedom for signal. The chosen approach was to use this information to produce one quantity for the tropospheric state: a "representative tropospheric VMR" (RTVMR), associated with an effective pressure. The effective pressure is an important quantity to consider in the interpretation of the results. The technique applied here could also be applied to other data sets, and could also be extended to data sets with significantly more than one degree of freedom for signal in the troposphere (with the caveat that there may be some overlap between the transformed averaging kernels for such data sets). Future work could also involve consideration of how best to make use of the fractional degrees of freedom for signal.

[39] TES RTVMRs were compared with output from the GEOS-Chem global chemical model. Our purpose was not to provide a validation of the TES methane product. However, the results shown demonstrate the potential of the existing TES $CH_4$ product for future scientific applications. The comparisons presented here verify that the latitudinal gradients observed in TES $CH_4$ data when used as suggested are representative of the real atmosphere rather than the a priori. Comparisons of TES with GEOS-Chem also point to large emissions of methane from enhanced biomass burning in Indonesia during the 2006 El Nino.

[40] **Acknowledgments.** The authors would like to thank the TES science team, particularly Susan Kulawik and Greg Osterman for providing information on the TES $CH_4$ retrievals and product status. These TES data were obtained from the NASA Langley Research Center Atmospheric Science Data Center. All TES data are available at http://eosweb.larc.nasa.gov/PRODOCS/tes/table_tes.html. We thank Yaping Xiao for providing $CH_4$ fields from her GOES-Chem simulations. We would also like to acknowledge the use of surface measurements from the NOAA Earth Systems Research Laboratory (ESRL) Global Monitoring Division (GMD) Carbon Cycle Greenhouse Gases (CCGG) program. These data are available at ftp://ftp.cmdl.noaa.gov/ccg/. Thanks also to Inna Megretskaia for help with the NOAA ESRL surface measurement analysis. This

work was funded by grants from NASA including grant NNX071B17G to Harvard University.

## References


Beer, R., T. A. Glavich, and D. M. Rider (2001), Tropospheric Emission Spectrometer for the Earth Observing System's Aura satellite, *Appl. Opt.*, *40*, 2356–2367, doi:10.1364/AO.40.002356.

Beer, R., et al. (2008), First satellite observations of lower tropospheric ammonia and methanol, *Geophys. Res. Lett.*, *35*, L09801, doi:10.1029/2008GL033642.

Bey, I., D. J. Jacob, R. M. Yantosca, J. A. Logan, B. Field, A. M. Fiore, Q. Li, H. Liu, L. J. Mickley, and M. Schultz (2001), Global modeling of tropospheric chemistry with assimilated meteorology: Model description and evaluation, *J. Geophys. Res.*, *106*, 23,073–23,096, doi:10.1029/2001JD000807.

Bowman, K. W., et al. (2006), Tropospheric Emission Spectrometer: Retrieval method and error analysis, *IEEE Trans. Geosci. Remote Sens.*, *44*(5), 1297–1306, doi:10.1109/TGRS.2006.871234.

Brasseur, G. P., D. A. Hauglustaine, S. Walters, P. J. Rasch, J.-F. Muller, C. Granier, and X. X. Tie (1998), MOZART, a global chemical transport model for ozone and related chemical tracers: 1. Model description, *J. Geophys. Res.*, *103*, 28,265–28,289, doi:10.1029/98JD02397.

Butler, T. M., P. J. Rayner, I. Simmonds, and M. G. Lawrence (2005), Simultaneous mass balance inverse modeling of methane and carbon monoxide, *J. Geophys. Res.*, *110*, D21310, doi:10.1029/2005JD006071.

Ceccherini, S., B. Carli, E. Pascale, M. Prosperi, P. Raspollini, and B. M. Dinelli (2003), Comparison of measurements made with two different instruments of the same atmospheric vertical profile, *Appl. Opt.*, *42*, 6465–6473, doi:10.1364/AO.42.006465.

Clerbaux, C., J. Hadji-Lazaro, S. Turquety, G. Mégie, and P.-F. Coheur (2003), Trace gas measurements from infrared satellite for chemistry and climate applications, *Atmos. Chem. Phys.*, *3*, 1495–1508.

Clough, S., et al. (2006), Forward model and Jacobians for Tropospheric Emission Spectrometer retrievals, *IEEE Trans. Geosci. Remote Sens.*, *44*(5), 1308–1323, doi:10.1109/TGRS.2005.860986.

Crevoisier, C., D. Nobileau, A. M. Fiore, R. Armante, A. Chedin, and N. A. Scott (2009), A new insight on tropospheric methane in the Tropics—First year from IASI hyperspectral infrared observations, *Atmos. Chem. Phys. Discuss.*, *9*, 6855–6887.

Deeter, M. N., et al. (2003), Operational carbon monoxide retrievals algorithm and selected results for the MOPITT instrument, *J. Geophys. Res.*, *108*(D14), 4399, doi:10.1029/2002JD003186.

De Mazière, M., et al. (2007), Validation of ACE-FTS v2.2 methane profiles from the upper troposphere to lower mesosphere, *Atmos. Chem. Phys. Discuss.*, *7*, 17,975–18,014.

Dlugokencky, E. J., B. P. Walter, K. A. Masarie, P. M. Lang, and E. S. Kasischke (2001), Measurements of an anomalous global methane increase during 1998, *Geophys. Res. Lett.*, *28*(3), 499–502, doi:10.1029/2000GL012119.

Dlugokencky, E. J., S. Houweling, L. Bruhwiler, K. A. Masarie, P. M. Lang, J. B. Miller, and P. P. Tans (2003), Atmospheric methane levels off: Temporary pause or a new steady-state?, *Geophys. Res. Lett.*, *30*(19), 1992, doi:10.1029/2003GL018126.

do Carmo, J. B., M. Keller, J. D. Dias, P. B. de Carmago, and P. Crill (2006), A source of methane from upland forests in the Brazilian Amazon, *Geophys. Res. Lett.*, *33*, L04809, doi:10.1029/2005GL025436.

Frankenberg, C., J. F. Meirink, M. van Weele, U. Platt, and T. Wagner (2005), Assessing methane emissions from global space-borne observations, *Science*, *308*(5724), 1010–1014, doi:10.1126/science.1106644.

Frankenberg, C., J. F. Merink, P. Bergamaschi, A. P. H. Goede, M. Heinmann, S. Koerner, U. Platt, M. van Weele, and T. Wagner (2006), Satellite chartography of atmospheric methane from SCIAMACHY on board ENVISAT: Analysis of the years 2003 and 2004, *J. Geophys. Res.*, *111*, D07303, doi:10.1029/2005JD006235.

Frankenberg, C., T. Warneke, A. Butz, I. Aben, F. Hase, P. Spietz, and L. R. Brown (2008a), Pressure broadening in the $2\nu3$ band of methane and its implication on atmospheric retrievals, *Atmos. Chem. Phys.*, *8*, 5061–5075.

Frankenberg, C., P. Bergamaschi, A. Butz, S. Houweling, J. F. Meirink, J. Notholt, A. K. Petersen, H. Schrijver, T. Warneke, and I. Aben (2008b), Tropical methane emissions: A revised view from SCIAMACHY onboard ENVISAT, *Geophys. Res. Lett.*, *35*, L15811, doi:10.1029/2008GL034300.

Intergovernmental Panel on Climate Change (IPCC) (2007), *Climate Change 2007: The Physical Science Basis—Fourth Assessment Report of the Intergovernmental Panel on Climate Change*, Cambridge Univ. Press, New York.

Joiner, J., and A. M. de Silva (1998), Efficient methods to assimilate remotely sensed data based on information content, *Q. J. R. Meteorol. Soc.*, *124*, 1669–1694, doi:10.1002/qj.49712454915.

Kulawik, S. S., J. Worden, A. Eldering, K. W. Bowman, M. Gunson, G. B. Osterman, L. Zhang, S. A. Clough, M. W. Shephard, and R. Beer (2006a), Implementation of cloud retrievals for Tropospheric Emission Spectrometer (TES) atmospheric retrievals: 1. Description and characterization of errors on trace gas retrievals, *J. Geophys. Res.*, *111*, D24204, doi:10.1029/2005JD006733.

Kulawik, S. S., G. B. Osterman, D. B. A. Jones, and K. W. Bowman (2006b), Calculation of altitude-dependent constraints for TES nadir retrievals, *IEEE Trans. Geosci. Remote Sens.*, *44*(5), 1334–1342, doi:10.1109/TGRS.2006.871206.

Kulawik, S. S., K. W. Bowman, M. Luo, C. D. Rodgers, and L. Jourdain (2008), Impact of nonlinearity on changing the a priori of trace gas profile estimates from the Tropospheric Emission Spectrometer (TES), *Atmos. Chem. Phys.*, *8*, 3081–3092.

Logan, J. A., I. A. Megretskaia, R. Nassar, L. T. Murray, L. Zhang, K. W. Bowman, H. M. Worden, and M. Luo (2008), The effects of the 2006 El Niño on tropospheric composition as revealed by data from the Tropospheric Emission Spectrometer (TES), *Geophys. Res. Lett.*, *35*, L03816, doi:10.1029/2007GL031698.

Nassar, R., P. F. Bernath, C. D. Boone, G. L. Manney, S. D. McLeod, C. P. Rinsland, R. Skelton, and K. A. Walker (2005), Stratospheric abundances of water and methane based on ACE-FTS measurements, *Geophys. Res. Lett.*, *32*, L15S04, doi:10.1029/2005GL022383.

Osterman, G., et al. (2008), Tropospheric Emission Spectrometer TES L2 data user's guide, version 3.1, Jet Propul. Lab., Calif. Inst. of Technol., Pasadena, Calif.

Pan, L., J. C. Gille, D. P. Edwards, and P. L. Bailey (1998), Retrieval of tropospheric carbon monoxide for the MOPITT experiment, *J. Geophys. Res.*, *103*(D24), 32,277–32,290, doi:10.1029/98JD01828.

Park, J. H., et al. (1996), Validation of halogen occultation experiments $CH_4$ measurements from the UARS, *J. Geophys. Res.*, *101*(D6), 10,183–10,203, doi:10.1029/95JD02736.

Park, M., W. J. Randel, D. E. Kinnison, R. R. Garcia, and W. Choi (2004), Seasonal variation of methane, water vapor and nitrogen oxides near the tropopause: Satellite observations and model simulations, *J. Geophys. Res.*, *109*, D03302, doi:10.1029/2003JD003706.

Payan, S., et al. (2007), Validation and data characteristics of methane and nitrous oxide profiles observed by MIPAS and processed with the Version 4.61 algorithm, *Atmos. Chem. Phys. Discuss.*, *7*, 18,043–18,111.

Randel, W. J., F. Wu, J. M. Russell, A. Roche, and J. W. Waters (1998), Seasonal cycles and QBO variations in stratospheric $CH_4$ and $H_2O$ observed in UARS HALOE data, *J. Atmos. Sci.*, *55*(2), 163–185, doi:10.1175/1520-0469(1998)055<0163:SCAQVI>2.0.CO;2.

Ravazi, A., C. Clerbaux, C. Wespes, L. Clarisse, D. Hurtmans, S. Payan, C. Camy-Peret, and P. F. Coheur (2009), Characterization of methane retrievals from the IASI space-borne sounder, *Atmos. Chem. Phys. Discuss.*, *9*, 7615–7643.

Rodgers, C. D. (2000), *Inverse Methods for Remote Sounding: Theory and Practice*, World Sci., Singapore.

Rodgers, C. D., and B. J. Connor (2003), Intercomparison of remote sounding instruments, *J. Geophys. Res.*, *108*(D3), 4116, doi:10.1029/2002JD002299.

Schoeberl, M. R., M. Z. Lu, and J. E. Rosenfield (1995), An analysis of the Antarctic Halogen Occultation Experiment trace gas observations, *J. Geophys. Res.*, *100*(D3), 5159–5172, doi:10.1029/94JD02749.

Smith, L. C., G. M. MacDonald, A. A. Velichko, D. W. Beilman, O. K. Borisova, K. E. Frey, K. V. Kremenetski, and Y. Sheng (2004), Siberian peatlands: A net carbon sink and global methane source since the early Holocene, *Science*, *303*, 353–356, doi:10.1126/science.1090553.

Steck, T., and T. von Clarmann (2001), Constrained profile retrieval applied to the observation mode of the Michelson Interferometer for Passive Atmospheric Sounding, *Appl. Opt.*, *40*, 3559–3571, doi:10.1364/AO.40.003559.

Susskind, J., C. D. Barnet, and J. M. Blaisdell (2003), Retrieval of atmospheric and surface parameters from AIRS/AMSU/HSB data in the presence of clouds, *IEEE Trans. Geosci. Remote Sens.*, *41*(2), 390–409.

Tikhonov, A. (1963), On the solution of incorrectly stated problems and method of regularization, *Dokl. Akad. Nauk SSSR*, *151*, 501–504.

Twomey, S. (1963), On the numerical solution of Fredholm integral equations of the first kind by the inversion of the linear system produced by quadrature, *J. ACM*, *10*, 97–101, doi:10.1145/321150.321157.

von Clarmann, T., and U. Grabowski (2007), Elimination of hidden a priori information from remotely sensed profile data, *Atmos. Chem. Phys.*, *7*, 397–408.

von Clarmann, T., et al. (2003), Retrieval of temperature and tangent altitude pointing from limb emission spectra recorded from space by the Michelson Interferometer for Passive Atmospheric Sounding (MIPAS), *J. Geophys. Res.*, *108*(D23), 4736, doi:10.1029/2003JD003602.

Wang, J. S., J. A. Logan, M. B. McElroy, B. N. Duncan, I. A. Megretskaia, and R. M. Yantosca (2004), A 3-D model analysis of the slowdown and interannual variability in the methane growth rate from 1988 to 1997, *Global Biogeochem. Cycles*, *18*, GB3011, doi:10.1029/2003GB002180.

Xiao, Y., D. J. Jacob, J. S. Wang, J. A. Logan, P. I. Palmer, P. Suntharalingam, R. M. Yantosca, G. W. Sachse, D. R. Blake, and D. G. Streets (2004), Constraints on Asian and European sources of methane from $CH_4$-$C_2H_6$-

CO correlations in Asian outflow, *J. Geophys. Res.*, *109*, D15S16, doi:10.1029/2003JD004475.

Xiong, X., C. Barnet, E. Maddy, C. Sweeney, X. Liu, L. Zhou, and M. Goldberg (2008), Characterization and validation of methane products from the Atmospheric Infrared Sounder (AIRS), *J. Geophys. Res.*, *113*, G00A01, doi:10.1029/2007JG000500.

S. A. Clough, Clough Radiation Associates, 89 Hancock Street, Lexington, MA 02420, USA.

J. A. Logan, School of Engineering and Applied Sciences, Harvard University, 108 Pierce Hall, 29 Oxford Street, Cambridge, MA 02138, USA.

R. Nassar, Centre for Global Change Science, University of Toronto, 60 George Street, Toronto, ON M5S 1A7, Canada.

V. H. Payne and M. W. Shephard, Atmospheric and Environmental Research, Inc., 131 Hartwell Avenue, Lexington, MA 02421, USA. (vpayne@aer.com)